Engineering Structures 323 (2025) 119268

Contents lists available at ScienceDirect

Engineering Structures

journal homepage: www.elsevier.com/locate/engstruct

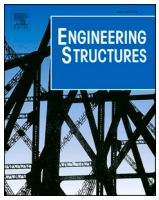

Analyzing the inelastic response of wind-excited steel tall buildings through a reduced-order model incorporating strength and stiffness degradation along with P-Delta effects

Jinghui Huang [a], Xinzhong Chen [b,*]

[a] Formerly, National Wind Institute, Department of Civil, Environmental and Construction Engineering, Texas Tech University, Lubbock, TX 79409–1023, USA
[b] President's Excellence in Research Professor, National Wind Institute, Department of Civil, Environmental and Construction Engineering, Texas Tech University, Lubbock, TX 79409–1023, USA

ARTICLE INFO

Keywords:
High-rise building
Reduced-order building model
Inelastic response
Stiffness degradation
Strength degradation
P-Delta effect
Wind-induced response
Wind loads

ABSTRACT

When wind-excited tall buildings undergo vibrations beyond their linear elastic range, it becomes imperative to account for both strength and stiffness degradation and P-Delta effects. This study investigates the influence of the degradation and P-Delta effects on the inelastic response of wind-excited tall buildings through a reduced-order building model, wherein the alongwind and crosswind building responses are presumed to be contributed by the fundamental modes. The backbone curves of the hysteretic relationships between the generalized restoring forces and displacements are developed through monotonic static modal pushover analysis utilizing a high-fidelity finite element building model with consideration of P-Delta effect. A cyclic modal pushover analysis is performed to ascertain the degradation of generalized building stiffness and strength in both translation directions, stemming from the deterioration of steel material in stiffness and strength. Subsequently, a biaxial hysteretic force model is employed to depict the hysteretic relationships between generalized forces and displacements, factoring in degradation and P-Delta effects. The inelastic response of a 60-story steel building subjected to both alongwind and crosswind load excitations is quantified through response history analysis to assess the accuracy of the reduced-order building model and to evaluate the influence of degradation of material strength and pre-yield stiffness and P-Delta effects on various responses.

1. Introduction

The inelastic performance of tall buildings under wind excitations has garnered growing research interest, particularly with the introduction of performance-based wind design permitting limited level of inelasticity [20,21,22,34,35,39,38,19,18,13,15,6,25,31,26,11,12,24,30,14]. Building models employed for analyzing inelastic response vary from a single-degree-of-freedom (SDOF) model to a more complex two-dimensional (2D) and three-dimensional (3D) multiple-degree-of-freedom (MDOF) nonlinear finite element (FE) models featuring distributed plasticity [32].

Huang and Chen [21] carried out inelastic response analysis of a 60-story steel building utilizing a reduced-order model. This model represented the building response through fundamental modal displacements. The hysteretic relations between the generalized restoring forces and displacements were established via static modal push-over analysis (MPA) employing a nonlinear FE building model. These relationships were then encapsulated with a biaxial hysteretic force model [42], wherein the restoring forces in two translational directions were interconnected and exhibited hysteretic behavior with building displacements in both directions. The accuracy of the reduced-order building model was validated against predictions of nonlinear FE model. The study presented a comprehensive analysis of alongwind and crosswind responses under uniaxial and biaxial wind loads at various wind speeds.

Experimental studies have demonstrated the significant strength and stiffness degradation during inelastic structural vibration, necessitating consideration when estimating inelastic response demand (e.g., [3,23,33,29]). Several modified hysteresis models, accounting for degradation or deterioration, have been developed. Baber and Noori [5] modified the original Bouc-Wen model [43,7] to include the component deterioration. Sivaselvan and Reinhorn [37] proposed a smooth hysteresis model

* Corresponding author.
E-mail addresses: jinghui.huang@ttu.edu (J. Huang), xinzhong.chen@ttu.edu (X. Chen).

https://doi.org/10.1016/j.engstruct.2024.119268
Received 14 March 2024; Received in revised form 3 October 2024; Accepted 31 October 2024
Available online 9 November 2024

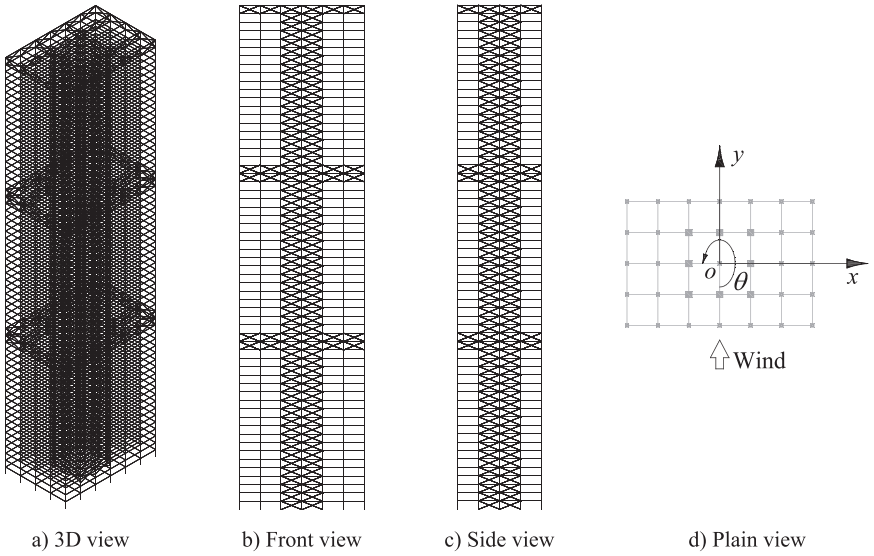

Fig. 1. FE model of the building frame.

with stiffness and strength degradation, incorporating pinching characteristics to describe inelastic material behavior. Gupta et al. [17] introduced a modified Clough-Johnston oscillator to get the correlations of strength and stiffness degradation, employing a simple damage index based on maximum displacement. Ibarra et al. [23] developed an energy-based hysteresis model capturing deterioration in strength and stiffness of building components, discussing three hysteresis models including bilinear, peak-oriented, and pinching models. Lignos and Keawinkler [29] explored the deterioration modeling of steel components based on an experimental database. The duration of strong wind loads, lasting for 2 to 4 h, significantly exceeds that of seismic loading. The degradation effect on wind-excited tall buildings can be potentially crucial and warrants investigation.

The P-Delta effect stands as another important consideration for tall buildings, as it has the potential to induce instability and building collapse. Gupta and Krawinkler [16] studied the P-Delta effect on flexible steel structures within the SAC Joint Venture project. Adam et al. [1] investigated the P-Delta effect for MDOF structures via equivalent SDOF systems, without considering degradation effect. Liang et al. [28] analyzed the response characteristics of an equivalent SDOF system while incorporating the P-Delta effect, comparing responses predicted using the same backbone curve but different hysteresis models, including nonlinear elastic model, the full elasto-plastic model and the Clough model. Yu et al., [45] investigated the P-Delta effect on the ductility demand of a 2DOF system under bidirectional seismic loads, incorporating the effects of strength and stiffness degradation through normalized hysteretic energy. Huang and Chen [20] explored the P-Delta effect on inelastic response of wind-excited tall buildings using nonlinear FE model.

This study investigates the inelastic response of a 60-story steel building subjected to both alongwind and crosswind load excitations, incorporating considerations for strength and stiffness degradation as well as P-Delta effect. A 2DOF reduced-order building model is established, wherein the alongwind and crosswind building responses are presumed to be contributed by the fundamental modes. The backbone curves of the hysteretic relations between the generalized restoring forces and displacements are developed through monotonic MPA, both without and with consideration of P-Delta effect, utilizing a FE building model. A cyclic MPA is performed to ascertain the degradation of generalized building stiffness and strength in both translation directions, stemming from the deterioration of steel material in stiffness and strength. Subsequently, a biaxial hysteretic force model is employed to depict the hysteretic relations between generalized forces and displacements, factoring in P-Delta and degradation effects. Utilizing this reduced-order building model, response statistics at various wind speeds, including time-varying mean, standard deviation (STD), kurtosis, and peak factors, are quantified through response history analysis (RHA). The accuracy of the reduced-order building model is assessed, and the degradation and P-Delta effects are evaluated. The new contributions from this study will be: 1) development of a reduced-order building model with a biaxial hysteresis that incorporates the influence of degradation of the generalized stiffness and strength resulted from the degradation of the steel material stiffness and strength, with a further consideration of the P-Delta effect; and 2) investigation of their effects on various building responses.

2. Nonlinear FE building model with degradation and P-Delta effects

In this study, a 60-story high-rise steel building with 182.88-m height, 45.72-m width, and 30.48-m depth is examined as an example (Fig. 1). The building has an outrigger system at three elevations: 20th and 21st floors, 40th and 41st floors and the 60th floor, alongside a core bracing system designed to withstand lateral load. The building frame comprises 2100 columns, 3480 beams, and 2560 diagonal bracings, including a total of 16 types of member sections. All members are modeled using fiber-type nonlinear element models [33], with each element featuring five fiber sections. Over 300 fibers are allocated per column and bracing cross-sectional area, and over 150 fibers per beam cross-sectional area. The typical column length is 3.048 m, and the typical beam length is 7.620 m. The structural mass was concentrated at the nodes, while the slabs are treated as rigid diaphragms. The fundamental modal frequencies in the two translational directions are estimated as $f_x = 0.173$ Hz and $f_y = 0.164$ Hz, with assumed modal damping ratios of $\zeta_x = \zeta_y = 1\%$. The fundamental mode shapes closely approximate linear variations. The torsional wind load and response are quite low thus are not considered. The mean wind speed is along y direction, resulting in $B = 45.72$ m and $D = 30.48$ m. Further detailed information about this FE model can be obtained from Park and Yeo and Huang and Chen [20].

To account for the P-Delta effect, the gravity load is defined as "dead load + 0.5 × live load", acting on all members. The dead load encompasses self-weight of the structure, dead slab load and super-imposed dead load.

The inelastic uniaxial stress-strain relation of the steel material is described by the following hysteretic Bouc-Wen model, which accounts

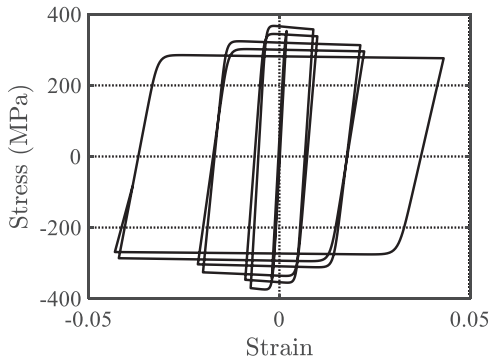

Fig. 2. Hysteretic relationship between strain and stress of the steel material.

for the degradation of initial stiffness and strength as proposed by Baber and Noori [5]. Additionally, this study introduces the consideration of degradation of second stiffness:

$$\sigma_s = \alpha_s(\epsilon_t)E\epsilon_s + (1-\alpha_s(\epsilon_t))Ez_s \tag{1a}$$

$$\dot{z}_s = \left[\dot{\epsilon}_s - (1+\delta_{\nu s}\epsilon_t)z_s I_s\right]/(1+\delta_{\eta s}\epsilon_s) \tag{1b}$$

$$I_s = |\epsilon_s||z_s|^{n-1}[\beta_{s0}+\gamma_{s0}\mathrm{sgn}(\dot{\epsilon}_s z_s)]\Big/\Delta_s^n \tag{1c}$$

$$\alpha_s(\epsilon_t) = \alpha_{s0}/(1+\delta_{\alpha s}\epsilon_t) \tag{1d}$$

$$\epsilon_t = \frac{1}{\Delta_s^2}\int_0^t (1-\alpha_s(\epsilon_t))\dot{\epsilon}_s z_s dt \tag{1e}$$

where σ_s and ϵ_s represent the stress and strain respectively; E denotes Young's modulus of elasticity; $\alpha_s(\epsilon)$ and α_{s0} represent the post-yield (second) stiffness ratios with and without consideration of degradation, with α_{s0} set to 0 in this study for steel material; $\delta_{\alpha s}$ is the parameter governing the degradation of the second stiffness, with a value of $\delta_{\alpha s}=0$ in this study for steel material; z_s is the hysteretic strain variable; Δ_s is the yield stress, set at Δ_s= 345 MPa; $\delta_{\nu s}$ is the parameter used for regulating strength degradation and $\delta_{\nu s}$ = 0.06; $\delta_{\eta s}$ is the parameter used to control the initial stiffness degradation and $\delta_{\eta s}$ = 0.035; ϵ_t is the normalized accumulative hysteretic energy; $n=6$ serves as the model shape parameter determining the smoothness of transition from pre-yielding to post-yielding region; and $\beta_0 = \gamma_0 = 0.5$. This material model is calibrated to replicate experimental data from a steel reduced beam section subjected to cyclic loading, as reported in Uang et al. [40].

This hysteretic model can be represented in the original Bouc-Wen model having degraded initial and second stiffness and strength, i.e., E', $\alpha_s'E'$ and Δ_s', which are functions of normalized accumulative hysteretic energy:

$$E'/E = (1+\delta_{\alpha s}\epsilon_t+\delta_{\eta s}\epsilon_t\alpha_s)/[(1+\delta_{\eta s}\epsilon_t)(1+\delta_{\alpha s}\epsilon_t)] \tag{2}$$

$$\Delta_s'/\Delta_s = 1\Big/(1+\delta_{\nu s}\epsilon_t)^{\frac{1}{n}} \tag{3}$$

$$\alpha_s'E'/\alpha_s E = 1/(1+\delta_{\alpha s}\epsilon_t) \tag{4}$$

Fig. 2 illustrates the hysteresis between strain and stress during cyclic strain. The normalized accumulated hysteretic energy ϵ is obtained through the integration of the hysteresis loops. For example, at $\epsilon_t = 30$, the ratio $E'/E = 0.49$ and the ratio $\Delta_s'/\Delta_s = 0.84$. Notably, the degradation of stiffness exceeds that of yield strength.

3. Wind loading model

The alongwind static wind force at the i-th story is determined as:

$$\overline{P}_i = 0.5\rho U_H^2 \overline{C}_D B H_0 \left(\frac{z_i}{H}\right)^{2\beta_s} \tag{5}$$

where ρ is the air density, 1.22 kg/m^3; U_H is the mean wind speed at the building top averaged in 10 min; B is the building width; H_0 is the story height and H_0 = 3.048 m; H is the building height; z_i is the elevation of i-th floor above the ground; $\overline{C}_D$ is the constant drag force coefficient and is determined from the static coefficient of base bending moment $\overline{C}_M$ as $\overline{C}_D = 2\overline{C}_M(\alpha_s+1)$; $\beta_s = 0.2$ is the power law exponent of the wind speed profile for the suburban terrain.

The cross power spectral density (CPSD) function between the i-th and the j-th story forces in alongwind direction is given as [8]:

$$S_{P_iP_j}(f) = S_{P_0}(f)\left(\frac{z_i}{H}\right)^{\beta_s}\left(\frac{z_j}{H}\right)^{\beta_s}\exp\left(-\frac{k_y f H}{U_H}\frac{|z_i-z_j|}{H}\right) \tag{6}$$

$$S_{P_0}(f) = \left(0.5\rho U_H^2 B H_0\right)^2 S_{C_M}(f)\Big/\left|\left(J_y(f)\right|\right|^2 \tag{7}$$

$$\left|\left(J_y(f)\right|\right|^2 = \left(\frac{H_0}{H}\right)^2\sum_{i=1}^{N}\sum_{j=1}^{N}\left(\frac{z_i}{H}\right)^{\beta_s+1}\left(\frac{z_j}{H}\right)^{\beta_s+1}\exp\left(-\frac{k_y f H}{U_H}\frac{|z_i-z_j|}{H}\right) \tag{8}$$

where $S_{C_M}(f)$ is the power spectrum of the base bending moment coefficient $C_M(t)$; $k_y = 7$ is the decay factor for the alongwind load; N is the number of stories and N = 60. Same CPSD model is also used for crosswind story forces, but different spectrum $S_{C_M}(f)$ and decay factor $k_y = 5$ are adopted. The power spectra density (PSD) of the alongwind and crosswind base bending moment coefficients follows the recommendations of the Architectural Institute of Japan (AIJ) [9,2]. For alongwind load, the STD σ_{C_M} is 0.110, while for crosswind load, it is 0.118; the bandwidth parameter of the spectrum takes $\beta_1 = 0.28$ with parameter κ_1 = 0.85, and the Strouhal number of S_t = 0.104. The alongwind and crosswind loads are considered mutually independent and simulated separately utilizing the power spectral models via spectral representation method [8,36].

4. Reduced-order building model with degradation and P-Delta effects

4.1. Biaxial hysteretic generalized restoring force model

The inelastic displacements of the building across its height in two directions closely resemble the fundamental mode shapes of the linear building model. Consequently, a 2DOF reduce-order nonlinear building model can be established, wherein the coupled equations for the generalized modal displacements are expressed as follows:

$$M_x\ddot{q}_x + 2M_x\zeta_x\omega_x\dot{q}_x + F_{sx}\left(q_x,\dot{q}_x,q_y,\dot{q}_y\right) = Q_x \tag{9a}$$

$$M_y\ddot{q}_y + 2M_y\zeta_y\omega_y\dot{q}_y + F_{sy}\left(q_x,\dot{q}_x,q_y,\dot{q}_y\right) = Q_y \tag{9b}$$

where q_x and q_y are the generalized modal displacements corresponding to the building top displacements in two directions; M_x, M_y ω_x, ω_y ζ_x and ζ_y are the generalized mass, modal frequencies and modal damping ratios of the linear building model; $F_{sx}\left(q_x,\dot{q}_x,q_y,\dot{q}_y\right)$ and $F_{sy}\left(q_x,\dot{q}_x,q_y,\dot{q}_y\right)$ are the generalized nonlinear hysteretic restoring forces; $Q_x(t)$ and $Q_y(t)$ are the generalized forces. When building response is within linear elastic range, $F_{sx}\left(q_x,\dot{q}_x,q_y,\dot{q}_y\right) = K_x q_x = M_x\omega_x^2 q_x$ and $F_{sy}\left(q_x,\dot{q}_x,q_y,\dot{q}_y\right) = K_y q_y = M_y\omega_y^2 q_y$, where K_x and K_y are the generalized modal stiffness, thus the equations reduces to uncoupled equations of linear modal displacements. However, when building surpasses the linear elastic range, the equations of motion become coupled, as the restoring

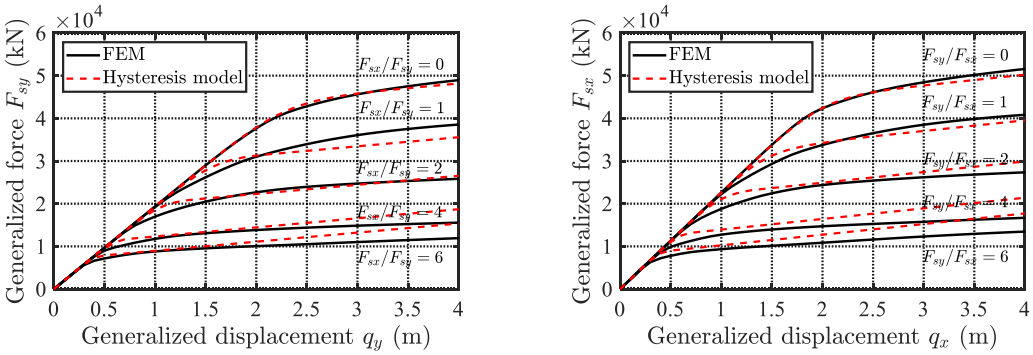

Fig. 3. Backbone curves of the generalized restoring force and displacement relations (without P-Delta, without degradation).

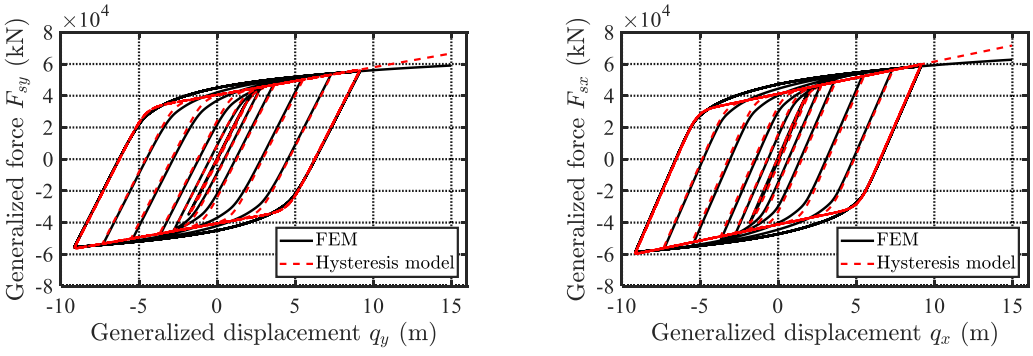

Fig. 4. Generalized restoring force and deformation relations under uniaxial cyclic loads (without P-Delta, without degradation).

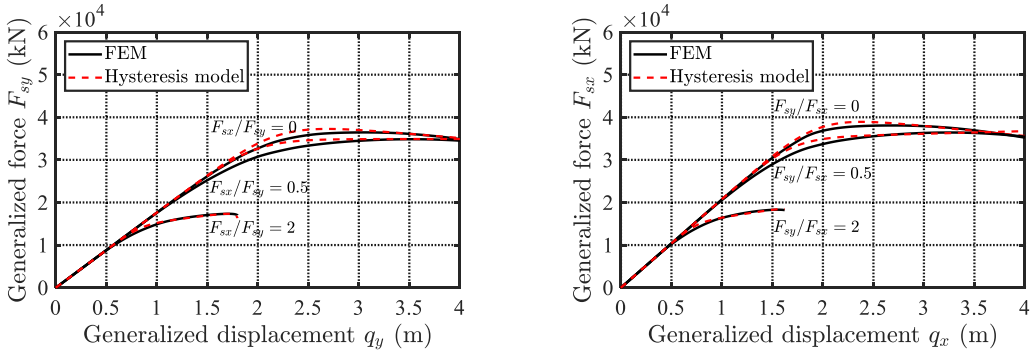

Fig. 5. Generalized restoring force and deformation relations under monotonic loads (with P-Delta, without degradation).

force in one direction is affected by the responses in both directions.

The relationships between the generalized restoring forces and displacements are quantified via static MPA procedure employing the nonlinear FE building model. These relationships are expressed as follows [27,41,44], where the degradation of the second stiffness is additionally incorporated in this study:

$$F_{sx} = \alpha_x(\epsilon)K_x q_x + [1-\alpha_x(\epsilon)]K_x z_x \tag{10a}$$

$$F_{sy} = \alpha_y(\epsilon)K_y q_y + [1-\alpha_y(\epsilon)]K_y z_y \tag{10b}$$

$$\dot{z}_x = \left[\dot{q}_x - (1+\delta_{\iota x}\epsilon)z_x I\right]/(1+\delta_{\eta x}\epsilon) \tag{11a}$$

$$\dot{z}_y = \left[\dot{q}_y - (1+\delta_{\eta y}\epsilon)z_y I\right]/(1+\delta_{\eta y}\epsilon) \tag{11b}$$

$$I = \left\{|\dot{q}_x||z_x|[\beta_0+\gamma_0 \mathrm{sgn}(\dot{q}_x z_x)]/\Delta_x^2 + \left|\dot{q}_y\right|\left|z_y\right|\left[\beta_0+\gamma_0 \mathrm{sgn}\left(\dot{q}_y z_y\right)\right]/\Delta_y^2\right\}$$

$$\times\left[(z_x/\Delta_x)^2+\left(z_y/\Delta_y\right)^2\right]^{\frac{n-2}{2}} \tag{11c}$$

$$\alpha_x(\epsilon) = \alpha_{x0}/(1+\delta_{\alpha x}\epsilon) \tag{11d}$$

$$\alpha_y(\epsilon) = \alpha_{y0}/(1+\delta_{\alpha y}\epsilon) \tag{11e}$$

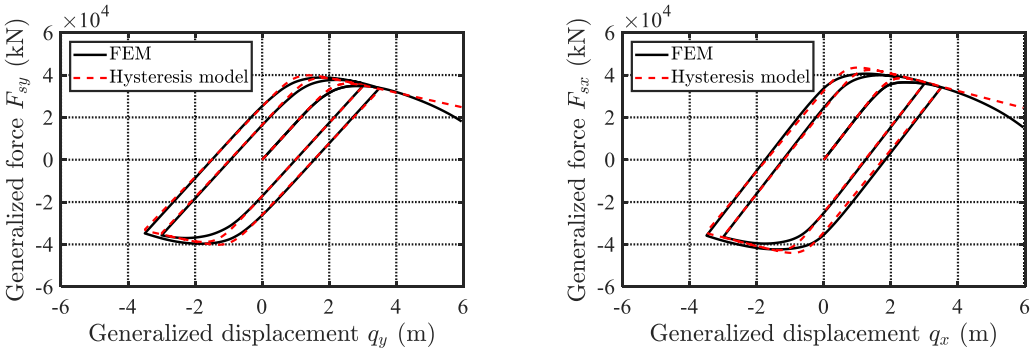

a) Alongwind (y) b) Crosswind (x)

Fig. 6. Generalized restoring force and deformation relations under cyclic loads (with P-Delta, without degradation).

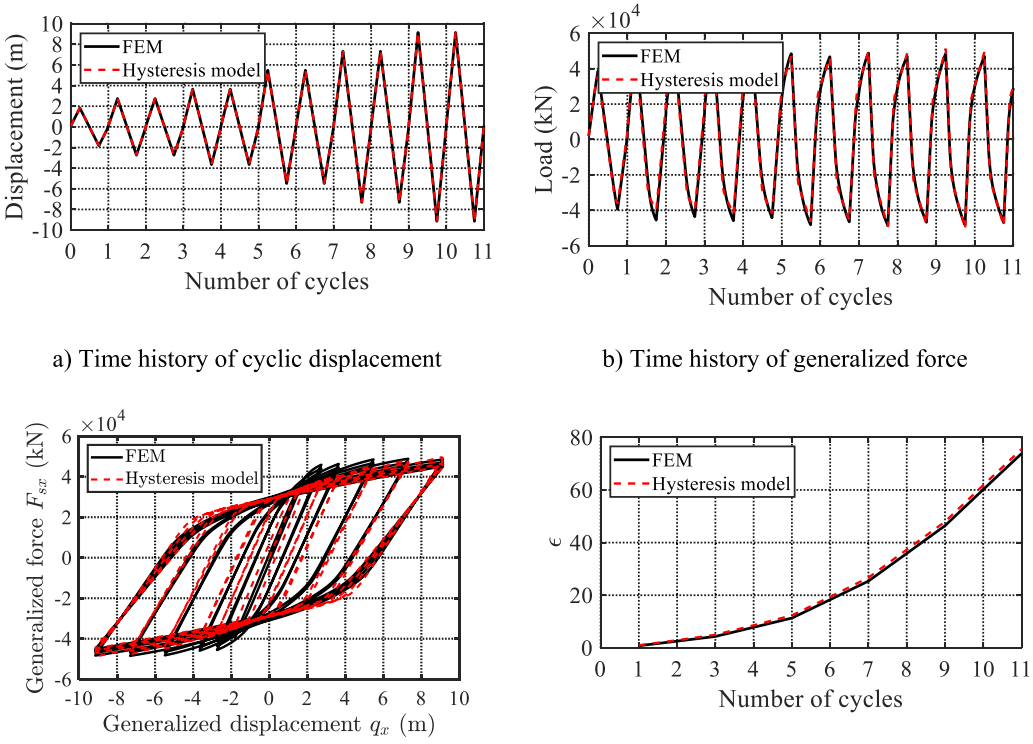

a) Time history of cyclic displacement b) Time history of generalized force

c) Generalized force-displacement relation d) Normalized accumulated hysteretic energy

Fig. 7. Generalized force and displacement relation under cyclic load in crosswind direction.

$$\epsilon = \int_0^t \left[(1-\alpha_x(\epsilon))\dot{q}_x z_x / \Delta_x^2 + (1-\alpha_y(\epsilon))\dot{q}_y z_y / \Delta_y^2 \right] dt \qquad (11\ \text{f})$$

where $\alpha_x(\epsilon)$ and $\alpha_y(\epsilon)$, α_{x0} and α_{y0}, are the second (post-yield stiffness ratios with and without effect of degradation; z_x and z_y are the hysteretic displacements; sgn(·) is the sign function; Δ_x and Δ_y are the generalized yield displacements under uniaxial loads in the x and y directions, respectively; ϵ is normalized hysteretic energy with respect to the largest elastic energy in each direction corresponding to the displacements Δ_x and Δ_y [27]; $\delta_{\nu x}$ and $\delta_{\nu y}$ are the parameters to control the strength degradation; $\delta_{\eta x}$ and $\delta_{\eta y}$ are the parameters controlling the degradation of initial stiffness; $\delta_{\alpha x}$ and $\delta_{\alpha y}$ are the parameters controlling the degradation of second stiffness; The shape parameter n determines the smoothness of transition from pre-yielding to post-yielding region; and $\beta_0 = \gamma_0 = 0.5$. When $\delta_{\nu x} = \delta_{\nu y} = \delta_{\eta x} = \delta_{\eta y} = \delta_{\alpha x} = \delta_{\alpha y} = 0$, this biaxial hysteretic model reduces to the original model without considering degradation.

4.2. *Hysteretic generalized forces without degradation and P-Delta effects*

Fig. 3 illustrates the backbone curves depicting the hysteretic generalized restoring force-displacement relations, determined through a monotonic MPA procedure employing the nonlinear FE building model (Huang and Chen 2023). Static loads in both translational x and y directions, following heightwise distributions of fundamental modal inertial loads, to the FE model. The load magnitudes are incrementally increased, and the corresponding building displacements are calculated. The generalized restoring forces F_{sx} and F_{sy} are computed from the distributed forces and modal shapes. The analysis is iterated for various combinations of F_{sx} and F_{sy}. When the load is applied solely in one direction, a uniaxial hysteretic relation between the restoring force and displacement is established. The normalized yield boundary from the FE

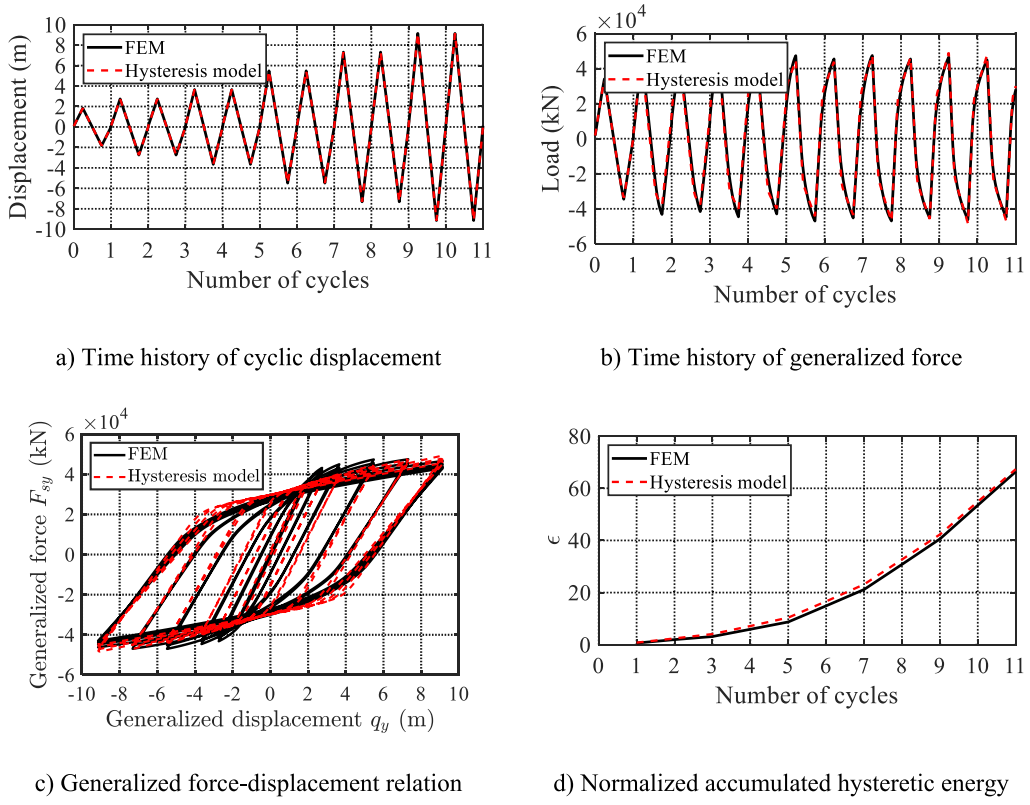

Fig. 8. Generalized force and displacement relations under cyclic load in alongwind direction.

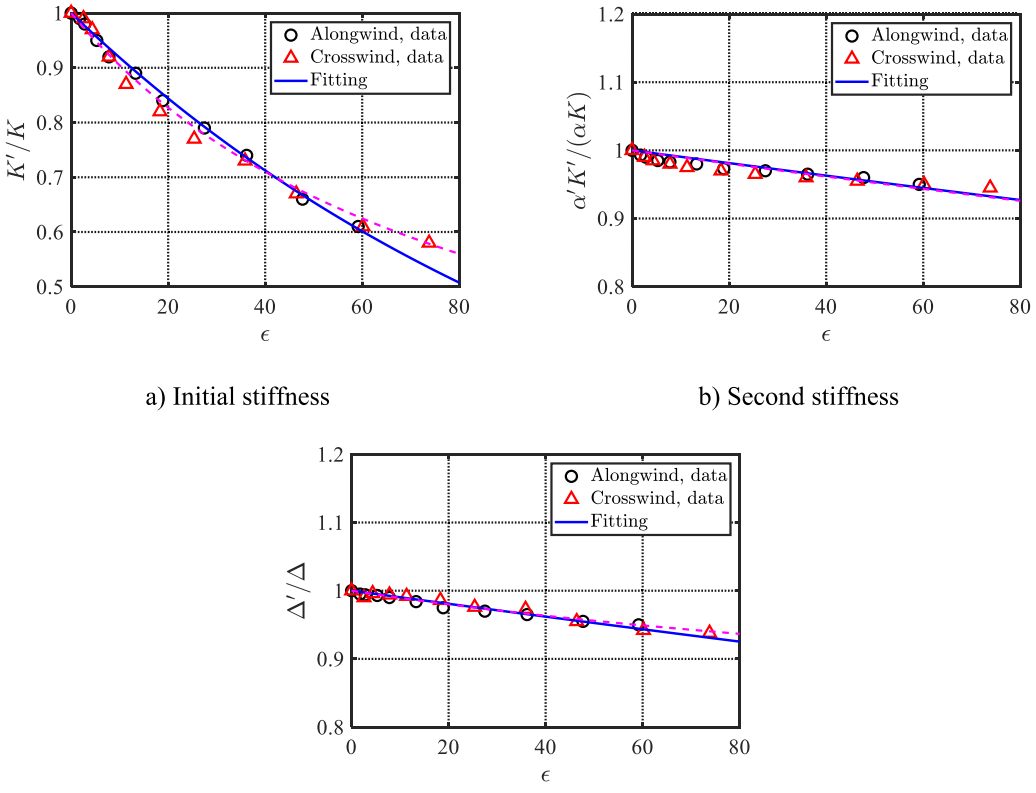

Fig. 9. Parameters of the hysteretic force model, accounting for degradation, as functions of hysteretic energy.

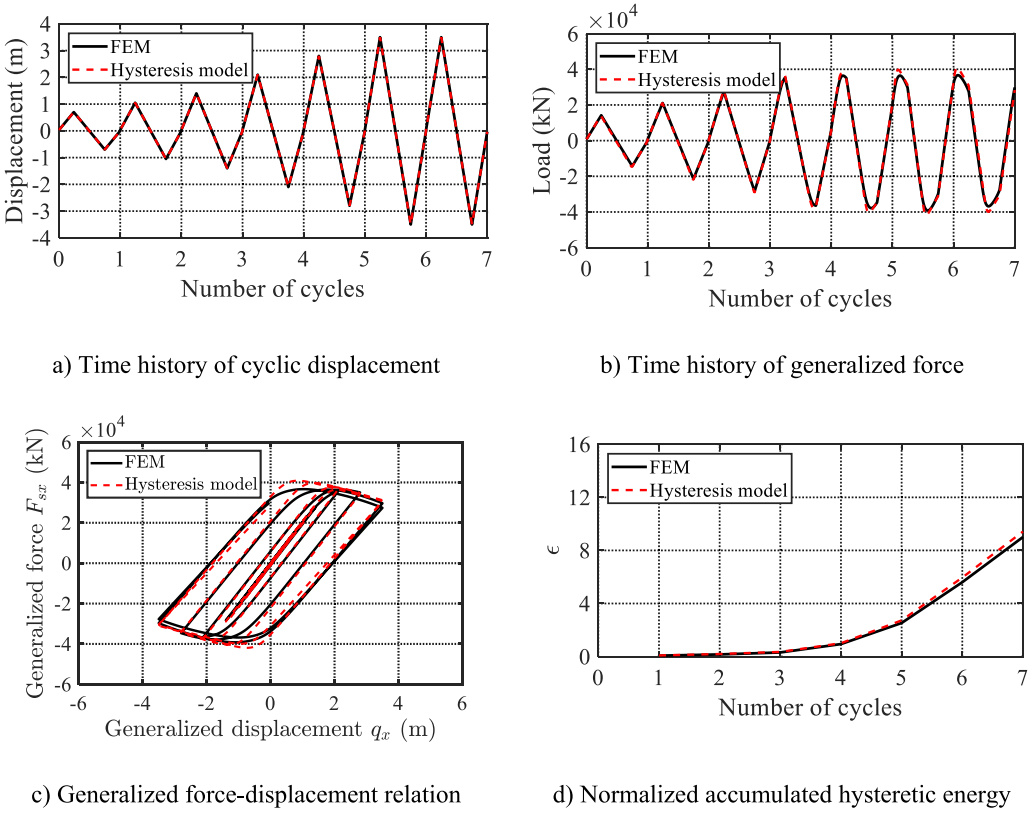

a) Time history of cyclic displacement

b) Time history of generalized force

c) Generalized force-displacement relation

d) Normalized accumulated hysteretic energy

Fig. 10. Generalized force and displacement relation under cyclic load in crosswind direction (with both P-Delta and degradation effects).

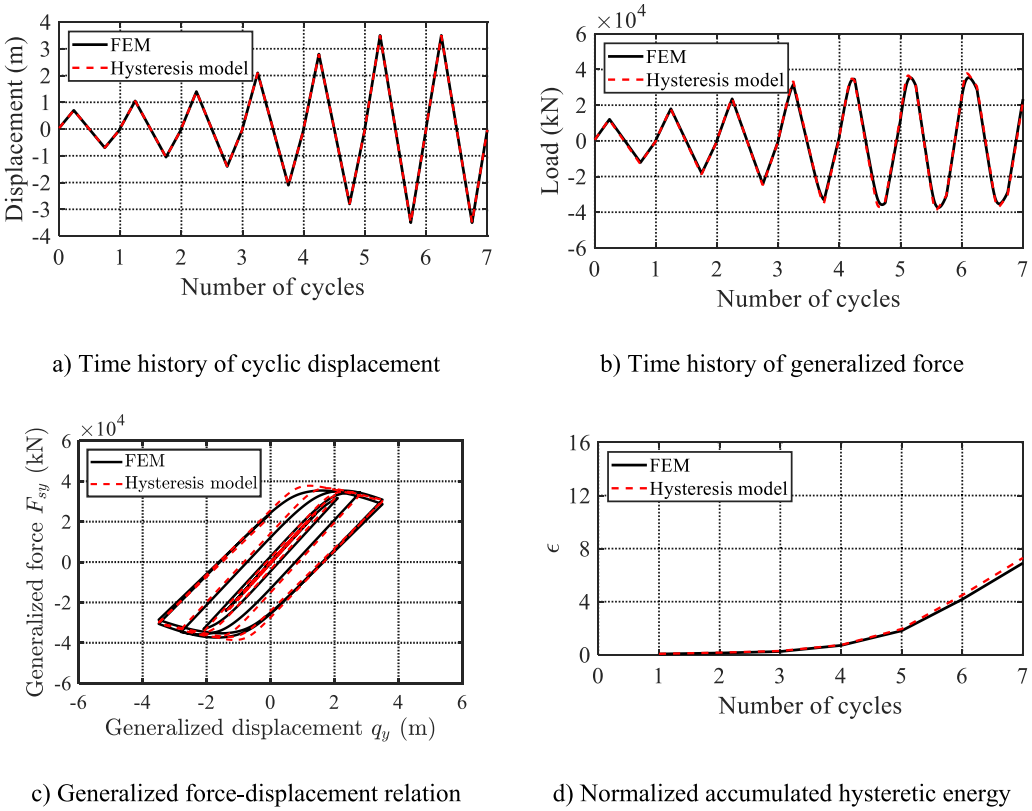

a) Time history of cyclic displacement

b) Time history of generalized force

c) Generalized force-displacement relation

d) Normalized accumulated hysteretic energy

Fig. 11. Generalized force and displacement relations under cyclic load in alongwind direction (with both P-Delta and degradation effects).

Table 1
Parameters of hysteretic force model.

P-Delta	Degradation	n	Δ_x	Δ_y	$\alpha_x = \alpha_y$	$\delta_{\nu x} = \delta_{\nu y}$	$\delta_{\eta x} = \delta_{\eta y}$	$\delta_{\alpha x} = \delta_{\alpha y}$
w/o	w/o	9	2.00	2.30	0.11	-	-	-
	w					0.01	0.012	0.001
w	w/o				−0.21	-	-	-
	w					0.07	0.02	0.02

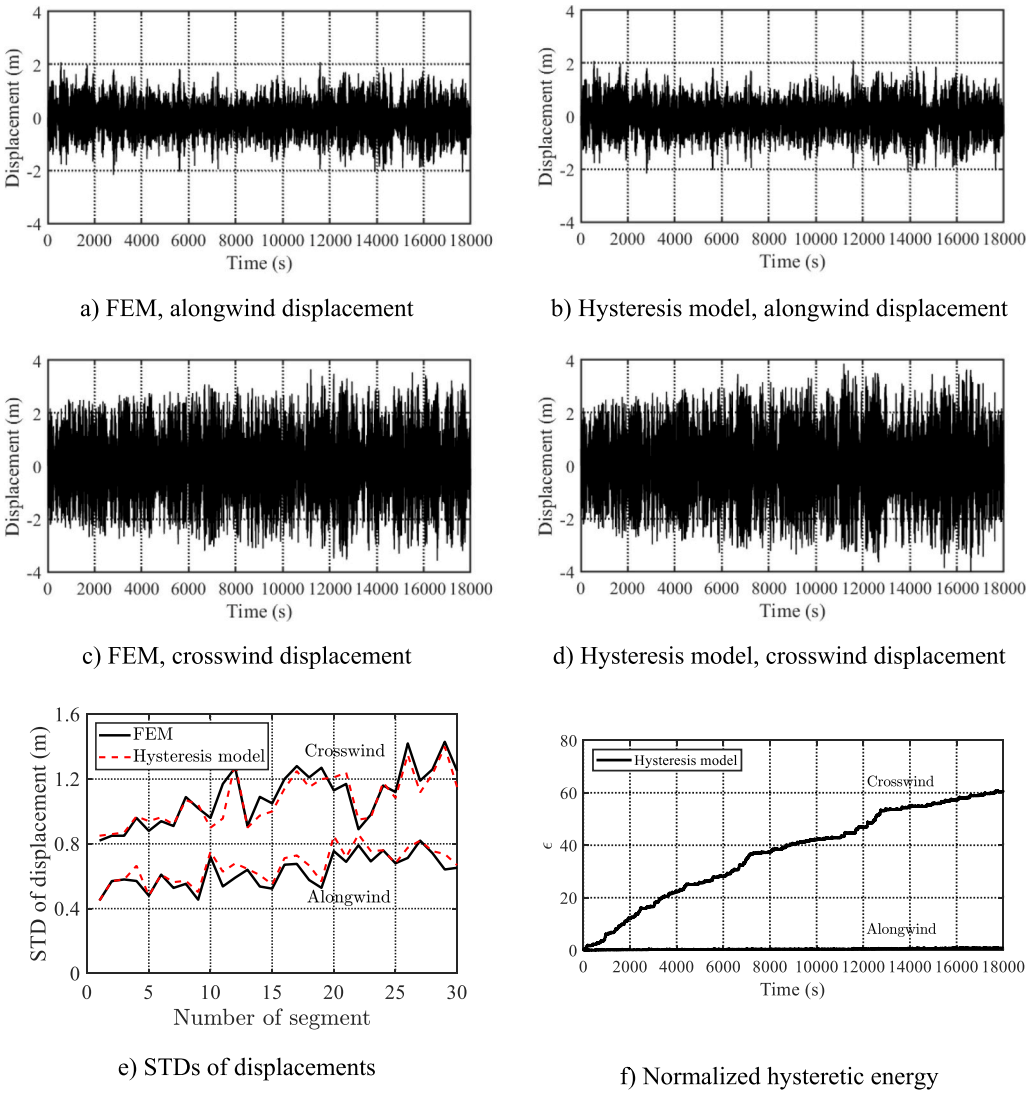

Fig. 12. Comparison of the statistics of building top displacements (Uniaxial loads).

model closely approximates a circle, indicating balanced interaction between the two directions. The biaxial hysteretic model is fitted with the following parameters: $K_x = 22,622$ kN/m, $K_y = 19,366$ kN/m, $n = 9$, $\alpha_x = \alpha_y = 0.11$, $\Delta_x = 2.0$m, and $\Delta_y = 2.3$m.

Fig. 4 displays the hysteresis loops of the uniaxial restoring force under progressively incremented cyclic displacement (See Figs. 7(a) and 8(a)) calculated from the FE model, alongside the fitted hysteresis model. The biaxial hysteresis model effectively captures the relationship between the generalized forces and displacements derived from the FE model, as evidenced by the agreement in the backbone curves and hysteresis rules.

4.3. Hysteretic generalized forces with P-Delta effect

Figs. 5 and 6 illustrates the relationships between the generalized forces and deformations obtained from the FE model using monotonic and cyclic MPA, considering the P-Delta effect. The uniaxial hysteretic models are fitted with the following parameters: $K_x = 20,773$ kN/m, $K_y = 17,627$ kN/m, $n = 9$, $\alpha_x = \alpha_y = -0.21$, $\Delta_x = 2.0$ m and $\Delta_y = 2.3$ m. The P-Delta effect causes a slight reduction in initial stiffness, a noticeable decrease in post-yield stiffness, but does not affect the yield displacements. Post-yield stiffness changes from positive to negative. The hysteresis model closely matches the results from the FE model. The P-Delta effect alters the backbone curve but does not affect the hysteresis rule. It can be effectively modeled by rotating the first and second stiffness of the original hysteretic model [1,10,4].

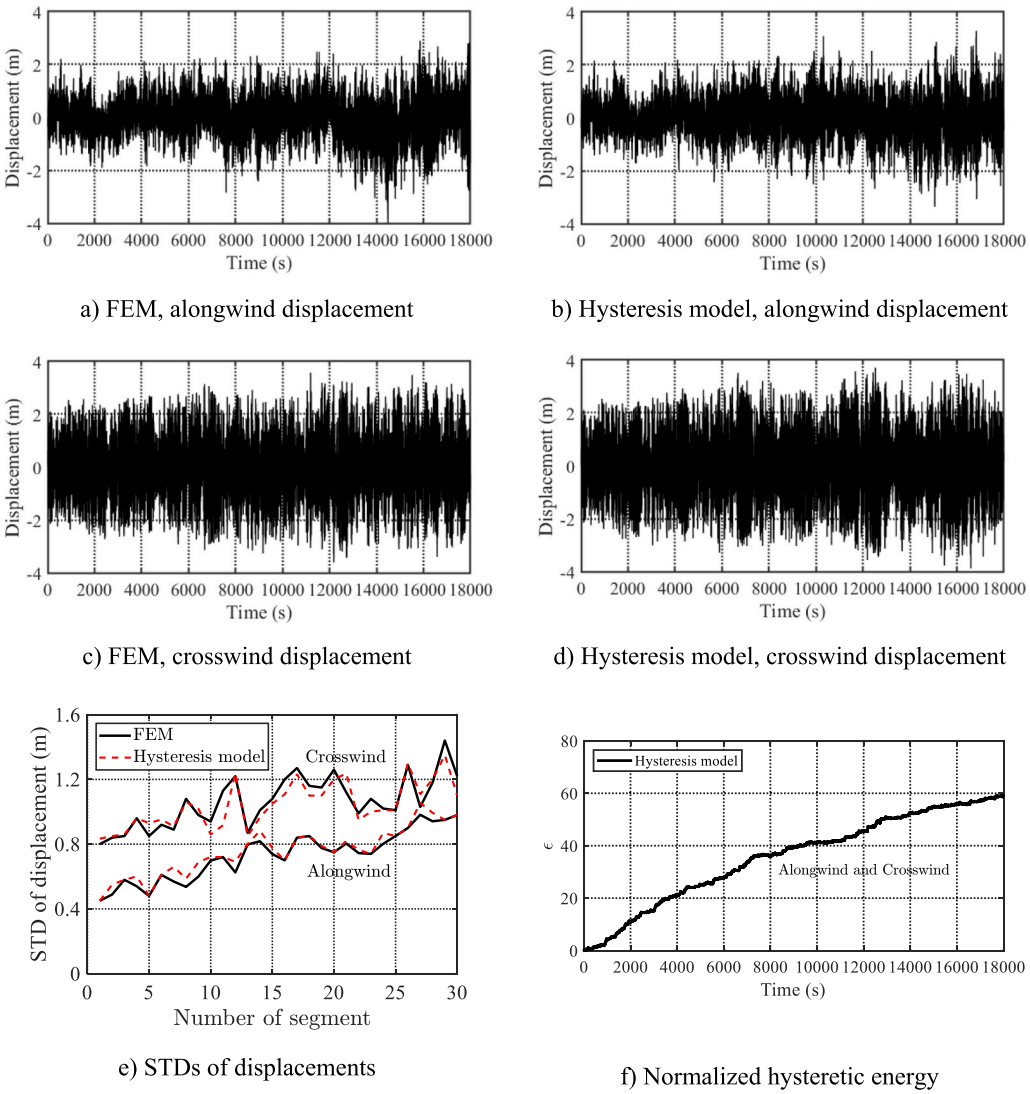

Fig. 13. Comparison of the statistics of building top displacements (Biaxial loads).

4.4. Hysteretic generalized forces with degradation effect

The hysteretic generalized force resulting from cyclic displacements of the building in a single direction was calculated using the material model incorporating degradation. Figs. 7 and 8 display the hysteretic generalized forces and progressively incremented cyclic displacements of the building applied separately in both directions. The normalized accumulated hysteretic energy levels over the cycles were also determined by integrating the hysteretic loops. For each cycle of hysteretic force in the FE model, a uniaxial Bouc-Wen hysteretic force model was fitted using a least-square fitting method with the model parameters (Zhu and Lu 2011): initial stiffness K'_x or K'_y, second stiffness $\alpha'_x K'_x$ or $\alpha'_y K'_y$, yield displacement Δ'_x or Δ'_y, and the parameter n.

Fig. 9 illustrates these model parameters as functions of hysteretic energy level ϵ, incorporating data for both alongwind and crosswind directions. The modal parameter n remains constant at 9. The first stiffness notably decreases with increasing hysteretic energy, while the degradations of strength and second stiffness are relatively minor. These model parameters are integrated into the following models as functions of energy (where the indices x and y are omitted for simplicity):

$$\alpha' K'/\alpha K = 1/(1+\delta_\alpha \epsilon) \tag{12}$$

$$K'/K = (1+\delta_\alpha \epsilon + \delta_\eta \epsilon \alpha)/[(1+\delta_\eta \epsilon)(1+\delta_\alpha \epsilon)] \tag{13}$$

$$\Delta'/\Delta = 1 \Big/ (1+\delta_\iota \epsilon)^{\frac{1}{n}} \tag{14}$$

which give $\delta_{\iota x} = \delta_{\nu y} = \delta_\nu = 0.010$, $\delta_{\eta x} = \delta_{\eta y} = \delta_\eta = 0.012$, and $\delta_{\alpha x} = \delta_{\alpha y} = \delta_\alpha = 0.001$. The hysteresis model, accounting for degradation, closely aligns with the FE data.

4.5. Hysteretic generalized forces with both degradation and P-Delta effects

Figs. 10 and 11 display the uniaxial hysteresis relationships, accounting for both P-Delta and degradation effects. The significance of the degradation effect increases with further consideration of the P-Delta effect is further considered. Table 1 provides a summary of the model parameters. Notably, without accounting for degradation, the P-Delta effect influences only the backbone curves and not the hysteresis rules.

5. Degradation effect on response statistics

5.1. Verification of reduced-order model with degradation

The effectiveness of reduced-order model, incorporating degradation

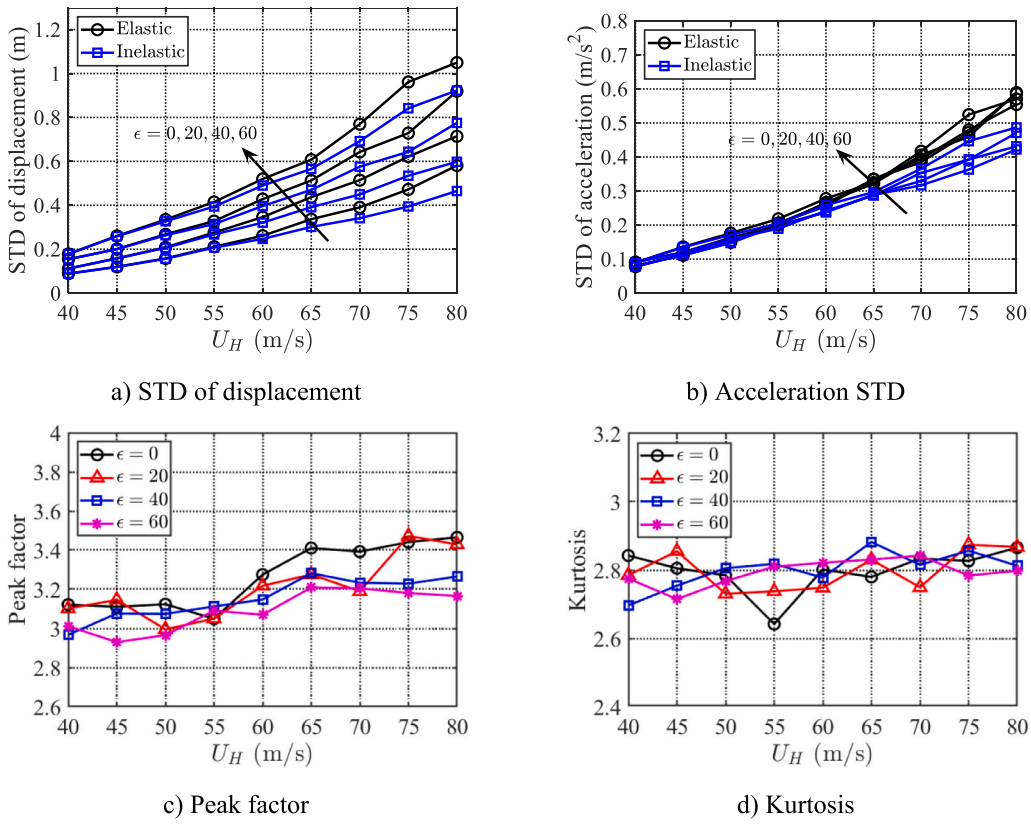

a) STD of displacement

b) Acceleration STD

c) Peak factor

d) Kurtosis

Fig. 14. Statistics of alongwind responses at various wind speeds and hysteretic energy levels.

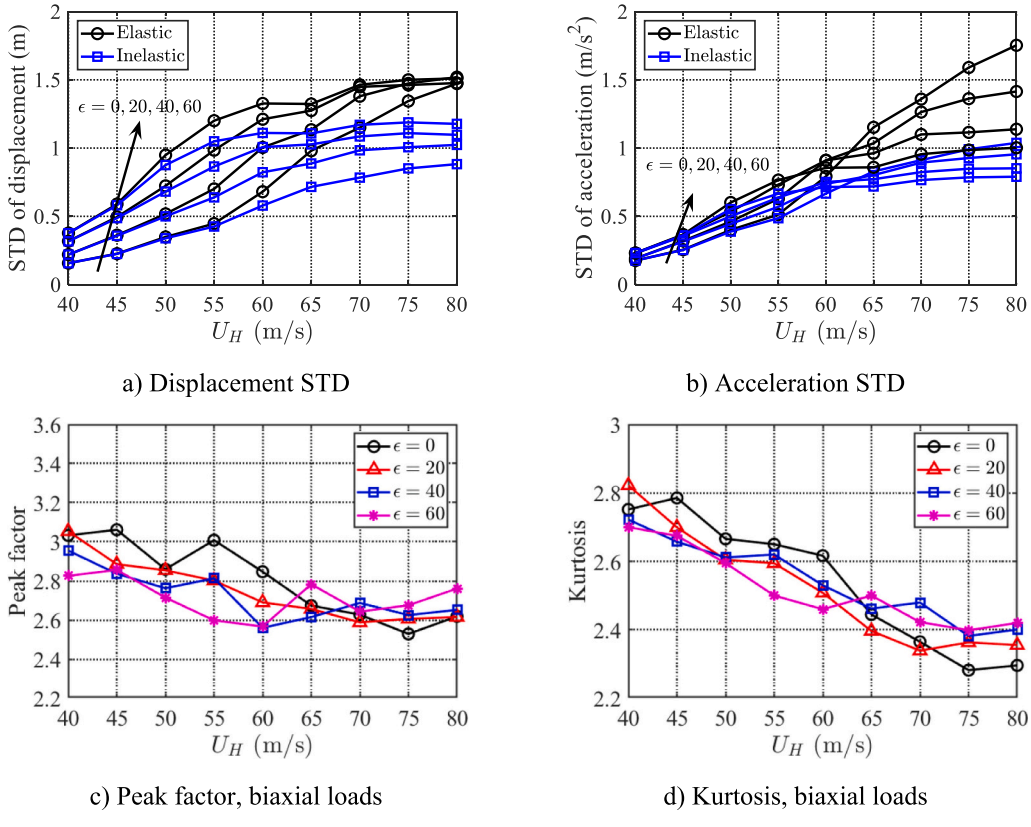

a) Displacement STD

b) Acceleration STD

c) Peak factor, biaxial loads

d) Kurtosis, biaxial loads

Fig. 15. Statistics of crosswind responses at various wind speeds and hysteretic energy levels.

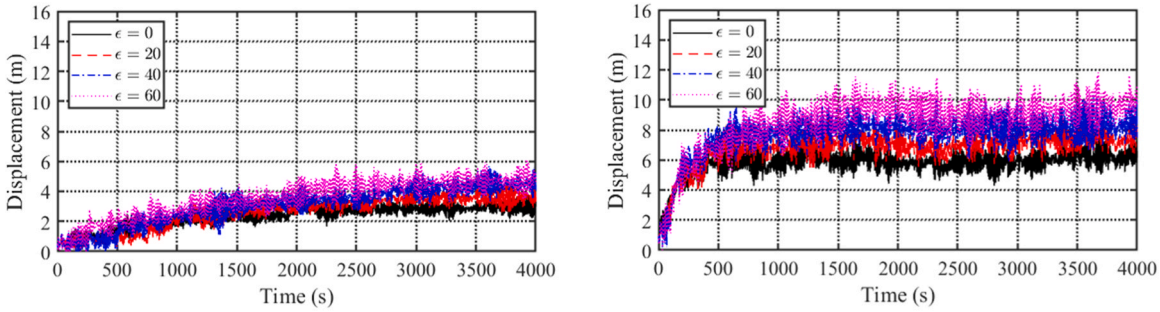

Fig. 16. Samples of alongwind building top displacement at various hysteretic energy levels.

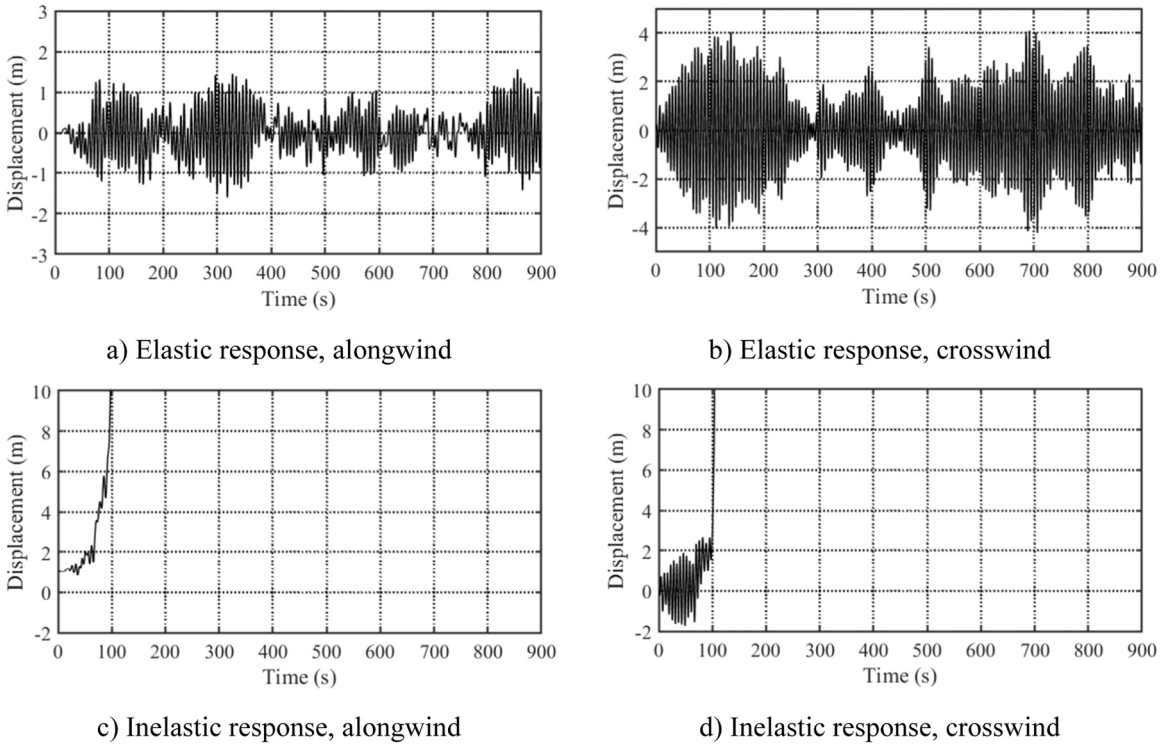

Fig. 17. Time history sample of the building top displacement with P-Delta effect ($U_H = 80$m/s, $\sigma_y = 345$ MPa).

but excluding the P-Delta effect, is evaluated through response history analysis and comparison with the results from the nonlinear FE model. Computation in the FE model is notably time-consuming, particularly when dealing with material hysteretic stress-strain relation and a large numbers of fiber sections and elements. The inelastic crosswind response under both uniaxial and biaxial loads at $U_H = 80$ m/s, with zero mean wind load, is computed for comparison. The response time history from the reduced-order model is calculated using the Runge-Kutta method, employing a time step of 0.04 s over a duration of 18,300 s. The initial 300 s is discarded to mitigate transient effect. The building is assumed to be initially at rest. The response time history of 18,300 s provides 30 sub-samples of response, each with a duration of 10 min, from which the STD of each sub-sample is estimated. The choice of storm duration of 18,000 s (i.e., 5 h) permits the investigation of the degradation effect over a wide range of accumulated normalized hysteretic energy, i.e., reaching a high level of 60. It should be noted that the mean alongwind load thus the time-varying mean alongwind displacement are not considered here but addressed in Section 5.3. As pointed out in [20], the existence of the time-varying mean alongwind displacement does not affect the fluctuating alongwind and crosswind responses.

Figs. 12 and 13 compare the time history, response STD and normalized hysteretic energy estimated from both the FE and reduced-order models. The reduced-order model demonstrates accurate prediction of the response STD. The degradation of stiffness and yield displacement leads to heightened inelastic response. While the biaxial effect diminishes the alongwind response, the degradation effect conversely increases it. Thus, with the consideration of degradation effect, the biaxial impact on alongwind response is mitigated.

5.2. *Effect of degradation on both alongwind and crosswind responses*

The effect of degradation on alongwind and crosswind response statistics is investigated using the reduced-order model. Both elastic and inelastic responses are computed for comparison. The 10-min mean wind speed at the building top ranges from $U_H = 40$ to 80 m/s. Initial accumulated hysteretic energy is specified at various levels (ϵ=0, 20, 40 and 60), determining the hysteresis model parameters with apparently reduced initial stiffness and only marginally decreased strength and

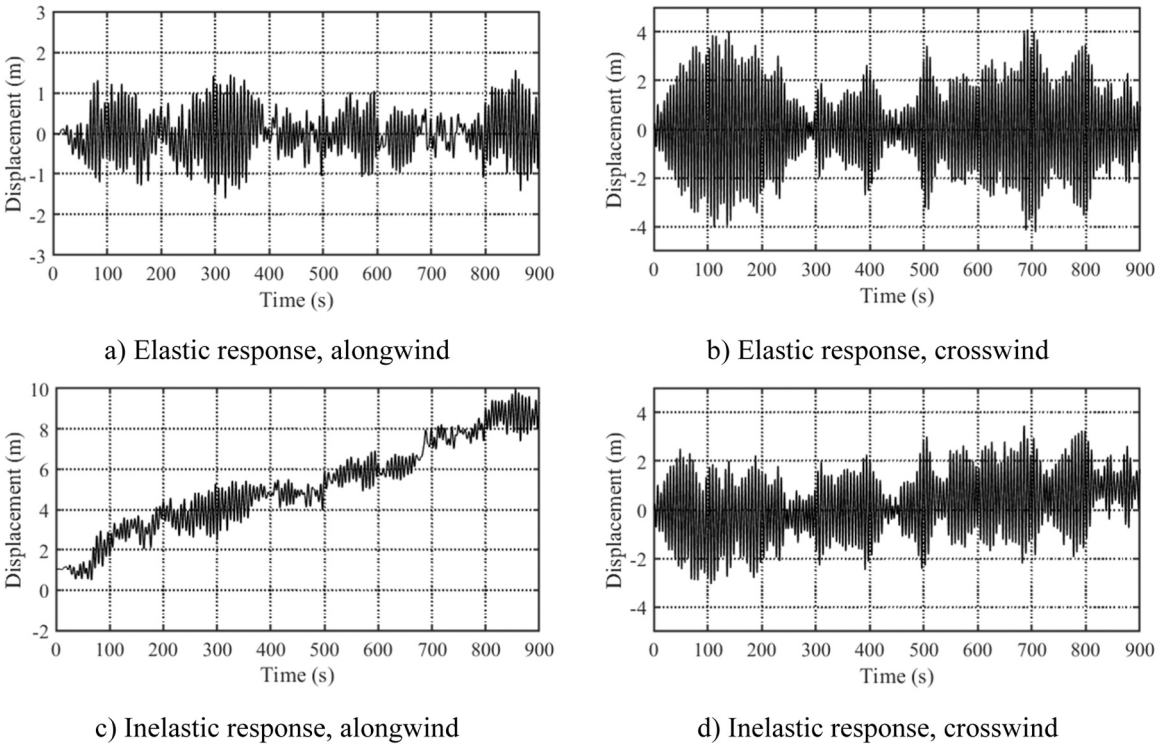

Fig. 18. Time history sample of the building top displacement with P-Delta effect (U_H = 80m/s, σ_y = 460 MPa).

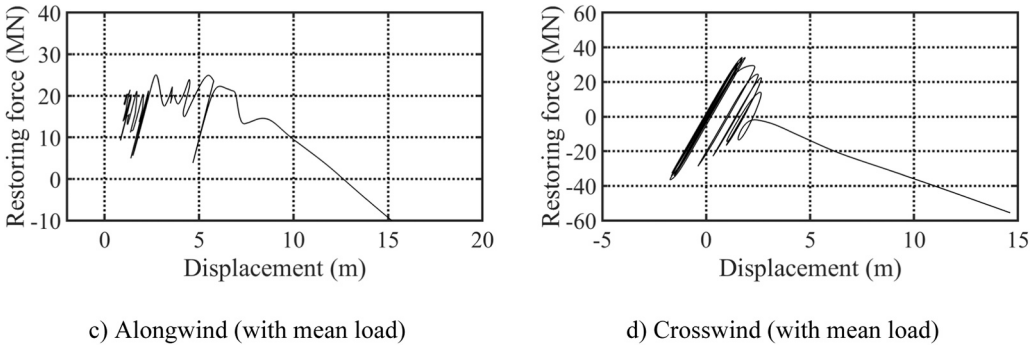

Fig. 19. Restoring force and displacement relations (with P-Delta) (U_H = 80m/s, σ_y = 345 MPa).

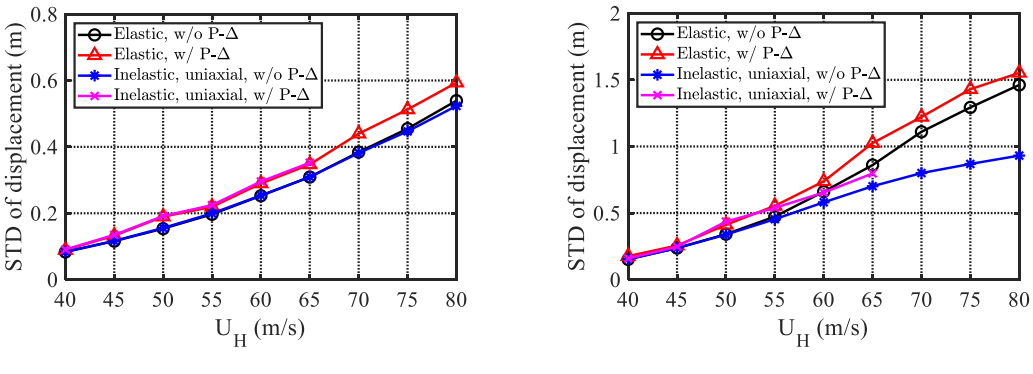

Fig. 20. STDs of building top displacements with P-Delta effect (σ_y = 345 MPa).

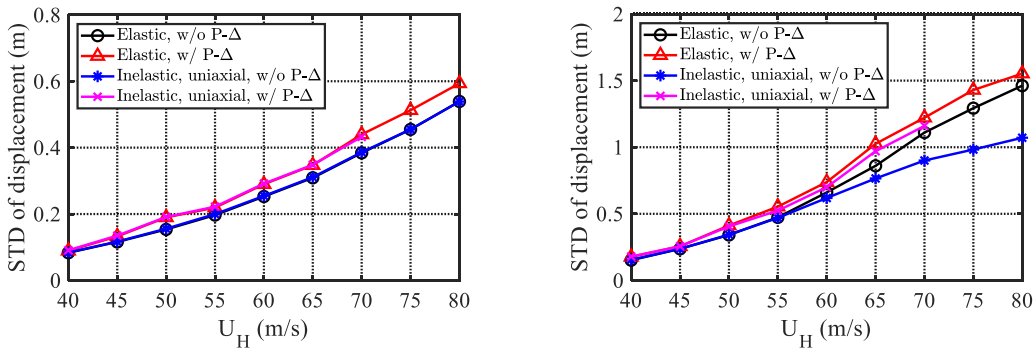

Fig. 21. STDs of building top displacements with P-Delta effect ($\sigma_y = 460$ MPa).

post-yielding stiffness. The accumulation of hysteretic energy within each 10 min is assumed to be negligibly small compared to the given initial energy level. The STD and other response statistics (kurtosis and peak factor) are calculated via ensemble average of 30 estimations.

Fig. 14 illustrates alongwind response results. It is observed that the degradation of stiffness notably increases the STD of alongwind displacement but has less influence on the STD of alongwind acceleration. The peak factor and kurtosis remain unaffected, indicating that the alongwind response maintains a Gaussian process.

Fig. 15 presents the crosswind response outcomes. The STDs of crosswind displacement and acceleration exhibit varying treads with increasing wind speed and change in stiffness. It is linked to the characteristics of the normalized crosswind loading power spectrum, which peaks at the vortex lock-in reduced wind speed, while as the alongwind load spectrum steadily rises with increasing reduced wind speed. With initial stiffness, the crosswind load spectrum peaks around wind speed of U_H= 80 m/s. With degradation of stiffness, the peak load is observed at a lower wind speed. The STD of elastic crosswind acceleration clearly depicts the characteristics of crosswind loading as wind speed increases. Besides the influence of spectral shape, degradation of stiffness predominantly affects crosswind displacement rather than acceleration. The crosswind response at higher wind speeds demonstrates evident hardening and non-Gaussian distribution with reduced peak factor and kurtosis, unaffected by the degradation of stiffness.

5.3. *Effect of degradation on time-varying mean alongwind displacement*

Fig. 16 illustrates alongwind displacement samples under biaxial loads, taking into account the mean alongwind load at U_H = 60 and 80 m/s while considering the degradation of stiffness. It is noted that the presence of mean alongwind load results in a time-varying mean component in the inelastic alongwind displacement. The steady-state displacement is governed by the mean wind load and post-yield stiffness in alongwind direction (Fang and Chen 2017 and 2018; Huang and Chen 2023). With a slight reduction in post-yield stiffness attributed to increased accumulated hysteretic energy, both transient and steady-state phases witness an increase in the time-varying mean alongwind displacement.

6. P-Delta effect on response statistics

Fig. 17 depicts the time histories of the alongwind and crosswind building top displacements with the P-Delta effect at U_H= 80 m/s, showcasing both linear elastic response and inelastic response calculated from the reduced-order model, with consideration of the mean alongwind load. Fig. 18 represents the response with yield stress of σ_y = 460 MPa using the same loading sample. Fig. 19 displays the relationship between restoring force and displacement relation. Figs. 20 and 21 portray the STDs of top displacements and accelerations at different wind speeds with yield stress values of σ_y = 345 MPa and 460 MPa.

It is evident that the P-Delta effect enhances the elastic response due to reduction in the pre-yield stiffness, where the mean wind speed is not greater than 55 m/s. In the case of inelastic response, the significant drift induced by the presence of mean wind load leads to a substantial P-Delta effect that could potentially result in building collapse. For the design of tall buildings, high-strength steel is generally used with yield stress from 460 MPa to 690 MPa, for which the P-Delta effect is unlikely to cause building collapse at higher wind speeds.

7. Conclusions

This research explored the inelastic behavior of a 60-story building under both alongwind and crosswind loads, utilizing a 2DOF reduced-order model. The model incorporated considerations for strength and stiffness degradation, as well as the P-Delta effect. A biaxial hysteretic force model was developed to depict the relations between generalized restoring forces and displacements, using modal pushover analysis with a detailed finite element building model accounting for P-Delta effect and steel material deterioration. Validation against the finite element model confirmed the accuracy of the reduced-order building model.

The pre-yield stiffness exhibited a significant decrease with heightened hysteretic energy, whereas the degradation of strength and post-yield stiffness remained relatively minor, stemming from material deterioration. Stiffness degradation notably increased the standard deviation of alongwind displacement but had less impact on alongwind acceleration statistics. Peak factor and kurtosis remained unchanged. A slight reduction in post-yield stiffness led to increased time-varying mean alongwind displacement during both transient and steady-state phases. Crosswind displacement was predominantly affected by stiffness degradation rather than acceleration. At higher wind speeds, crosswind response showed hardening and non-Gaussian distribution with reduced peak factor and kurtosis, unaffected by stiffness degradation.

The P-Delta effect caused a slight reduction in pre-yield stiffness and a noticeable decrease in post-yield stiffness without affecting yield displacements. It altered the backbone curve but not the hysteresis rule of generalized restoring force-displacement relationships. Significant alongwind displacement drift induced by mean wind load at higher speeds resulted in substantial P-Delta effects potentially leading to building collapse. However, high-strength steel design mitigated this effect, reducing the risk of collapse at higher wind speeds.

CRediT authorship contribution statement

Jinghui Huang: Writing – original draft, Software, Formal analysis, Data curation. **Xinzhong Chen:** Writing – review & editing,

Supervision, Methodology.

Declaration of Competing Interest

The authors declare that they have no known competing financial interests or personal relationships that could have appeared to influence the work reported in this paper.

Acknowledgements

The support for this work provided in part by the National Science Foundation (NSF) grant No. CMMI-2153189 is greatly acknowledged.

Data Availability

Data will be made available on request.

References

[1] Adam C, Ibarra LF, Krawinkler H. Evaluation of P-Delta effects in non-deteriorating MDOF structures from equivalent SDOF systems. Proc, 13th World Conf Earthq Eng, Vanc, B C, Can 2004;3407.
[2] Architectural Institute of Japan (AIJ). (2015). AIJ recommendations for load on buildings. Tokyo, AIJ.
[3] American Society of Civil Engineers (ASCE).(2017). Minimum design loads and associated criteria for buildings and otherstructures. Reston, VA, ASCE.
[4] ATC. Seismic evaluation and retrofit of concrete buildings. Redwood City: Seismic Safety Commission,; 1996.
[5] Baber TT, Noori MN. Random vibration of degrading, pinching systems. J Eng Mech 1985;111(8):1010–26.
[6] Beck AT, Kougioumtzoglou IA, dos Santos KR. Optimal performance-based design of non-linear stochastic dynamical RC structures subject to stationary wind excitation. Eng. Struct. 2014;78:145–53.
[7] Bouc, R. (1967). Forced vibrations of mechanical systems with hysteresis. In Proc. 4th conference on nonlinear oscillations, Prague.
[8] Chen X, Kareem A. Proper orthogonal decomposition-based modeling, analysis, and simulation of dynamic wind load effects on structures. J Eng Mech 2005;131(4):325–39.
[9] Ding J, Chen X. Fatigue damage evaluation of broad-band Gaussian and non-Gaussian wind load effects by a spectral method. Probab Eng Mech 2015;41:139–54.
[10] FEMA. Prestandard and commentary for the seismic rehabilitation of buildings. Washington D.C: Federal Emergency Management Agency,; 2000.
[11] Feng C, Chen X. Crosswind responses of tall buildings with nonlinear aerodynamic damping and hysteretic restoring force character. J. Wind Eng. Ind. Aerodyn. 2017;167:62–74.
[12] Feng C, Chen X. Inelastic responses of wind-excited tall buildings: Improved estimation and understanding by statistical linearization approaches. Eng. Struct. 2018;159:141–54.
[13] Gani F, Légeron F. Relationship between specified ductility and strength demand reduction for single degree-of-freedom systems under extreme wind events. J. Wind Eng. Ind. Aerodyn. 2012;109:31–45.
[14] Ghaffary A, Moustafa MA. Performance-based assessment and structural response of 20-story sac building under wind hazards through collapse. J. Struct. Eng. 2021;147(3):04020346.
[15] Griffis L., Patel V., Muthukumar S., Baldava S. A framework for performance-based wind engineering. Advances in hurricane engineering. Miami, Florida, USA; 2013. p. 1205–1216.
[16] Gupta A, Krawinkler H. Dynamic P-delta effects for flexible inelastic steel structures. J Struct Eng 2000;126(1):145–54.
[17] Gupta VK, Nielsen SR, Kirkegaard PH. A preliminary prediction of seismic damage-based degradation in RC structures. Earthq Eng Struct D 2001;30(7):981–93.
[18] Hart GC, Jain A. Performance-based wind evaluation and strengthening of existing tall concrete buildings in the Los Angeles region: Dampers, nonlinear time history analysis and structural reliability. Struct. Des. Tall Spec. Build. 2014;23(16):1256–74.
[19] Hong HP. Accumulation of wind induced damage on bilinear SDOF systems. Wind Struct. 2004;7(3):145–58.
[20] Huang JH, Chen X. Inelastic performance of high-rise buildings to simultaneous actions of alongwind and crosswind loads. J Struct Eng 2022;148(2):04021258.
[21] Huang JH, Chen X. Inelastic response of high-rise buildings under strong winds: Accuracy of reduced-order building model and influence of biaxial response interaction. J Struct Eng 2023;149(1):04022211.
[22] Huang JH, Chen X. Uncertainty analysis of inelastic response of high-rise buildings to wind using a reduced-order building model. Eng Struct 2023;288:116224.
[23] Ibarra LF, Medina RA, Krawinkler H. Hysteretic models that incorporate strength and stiffness deterioration. Earthq Eng Struct D 2005;34(12):1489–511.
[24] Judd JP. Windstorm resilience of a 10-story steel frame office building. ASCE-ASME J. Risk Uncertainty Eng. Syst., Part A: Civ. Eng. 2018;4(3):04018020.
[25] Judd JP, Charney FA. Inelastic behavior and collapse risk for buildings subjected to wind loads. Portland, USA: Structures Congress; 2015. p. 2483–96.
[26] Judd JP, Charney FA. Wind performance assessment of buildings. In: Geotechnical and Structural Engineering Congress; 2016. p. 1259–68.
[27] Lee CS, Hong HP. Statistics of inelastic responses of hysteretic systems under bidirectional seismic excitations. Eng Struct 2010;32(8):2074–86.
[28] Liang R, Wu J, Ge H, Wang C. Hysteretic characteristic with P-Δ effect and its influence on collapse resistance capacity of structure under earthquakes. J Earthq Tsunami 2013;7(03):1350022.
[29] Lignos DG, Krawinkler H. Deterioration modeling of steel components in support of collapse prediction of steel moment frames under earthquake loading. Journal of Structural Engineering 2011;137(11):1291–302.
[30] Mohammadi A, Azizinamini A, Griffis L, Irwin P. Performance assessment of an existing 47-story high-rise building under extreme wind loads. J. Struct. Eng. 2019;145(1):04018232.
[31] Mooneghi, M. A., Irwin, P., and Chowdhury, A. G. (2015). Exploratory studies on a bilinear aeroelastic model for tall buildings. Proc., 14th Int. Conf. Wind Eng., Porto Alegre, Brazil.
[32] NIST (2010). Nonlinear structural analysis for seismic design: A guide for practicing engineers. NIST GCR 10–917-5. Gaithersburg, MD.
[33] NIST (2017). Guidelines for nonlinear structural analysis for design of buildings. Part I-General. NIST GCR 17–917-46v1. Gaithersburg, MD.
[34] Ohkuma T, Kurita T, Ninomiya M. Response estimation based on energy balance for elasto-plastic vibration of tall building in across-wind direction. Proc., 7th Int. Conf. on Struct. Saf. and Reliab., Kyoto, Japan 1997:1359–66.
[35] Ouyang Z, Spence SM. Performance-based wind-induced structural and envelope damage assessment of engineered buildings through nonlinear dynamic analysis. J. Wind Eng. Ind. Aerodyn. 2021;208:104452.
[36] Shinozuka M, Jan CM. Digital simulation of random processes and its applications. J Sound Vib 1972;25(1):111–28.
[37] Sivaselvan MV, Reinhorn A. Hysteretic models for deteriorating inelastic structures. Journal of Engineering Mechanics 2000;126(6):633–40.
[38] Tamura Y, Yasui H, Marukawa H. Non-elastic responses of tall steel buildings subjected to across-wind forces. Wind Struct. 2001;4(2):147–62.
[39] Tsujita O, Hayabe Y, Ohkuma T. A study on wind-induced response for inelastic structure. Proc., 7th Int. Conf. on Struct. Saf. and Reliab., Kyoto, Japan 1997:1359–66.
[40] Uang, C.M., Yu, Q.S., and Gilton, C.S. (2000). Effects of loading history on cyclic performance of steel RBS moment connections. In Proc. 12th WCEE, Upper Hutt, New Zealand.
[41] Wang CH, Chang SY. Development and validation of a generalized biaxial hysteresis model. J Eng Mech 2007;133(2):141–52.
[42] Wang CH, Wen YK. Evaluation of pre-northridge low-rise steel buildings. I: modeling. J Struct Eng 2000;126(10):1160–8.
[43] Wen YK. Method for random vibration of hysteretic systems. J Eng Mech Div 1976;102(2):249–63.
[44] Wen YK. Methods of random vibration for inelastic structures. Appl Mech Rev 1989;42(2):39–52.
[45] Yu B, Yang L, Li B. P-Δ effect on probabilistic ductility demand and cumulative dissipated energy of hysteretic system under bidirectional seismic excitations. J Eng Mech 2014;141(4):04014141.